CHAPTER 8

Mechanical and Wear Properties of Compo-Cast SiO_2 Coated ABO_w/ Al-319 Composites

Al-319 matrix composite reinforced with varying percentages (2.5, 5, 7.5, 10 wt%) of SiO_2- coated $Al_{18}B_4O_{33}$ whiskers were fabricated by compo-casting technique. SiO_2 coating of whiskers was given by hydrolyzation method. The coating content effect on the whiskers/matrix microstructures and tribological properties of the composites were examined using scanning electron microscopy (SEM), XRD, transmission electron microscopy (TEM) and energy dispersive spectrometry (EDS). Scanning probe microscopy (SPM) was used for worn surface analysis of composite. A transition from mild to severe wear under high load applications ranging from 10 to 40 N took place due to fracture of whiskers and severe interfacial cracking. Compared with the cast composite, the whisker reinforced composite has lower wear resistance due to weak whisker/matrix interface and lowered whisker strength. An increase in coefficient of friction and wear rate was induced due to deep surface damage on increasing the sliding speed at lower applied loads. An increase in sliding speed further led to the strain hardening of the subsurface layer and Al_2O_3 layer formation on worn surface, leading to a decrease in friction and wear rate coefficient.

Additionally, stirring parameters of compo-casting were also studied. The whisker distribution in composites was used to determine stirring parameters. Compo casting stirring was used to fabricate the composites with homogeneously distributed whiskers at 600 °C for 30 min. The wear results of ABO_w/SiO_2/Al-319 composite is up by 7.5% by that of composite. The interfacial product Al_2O_3 resulting from the reaction

between the liquid Al-Cu and the SiO_2 coating enhances the interfacial bond strength, thus increasing the load transfer to reinforcement from matrix, leading to better wear properties in composites.

8.1. Characterization of SiO_2 coated and uncoated $Al_{18}B_4O_{33w}$

Figure 8.1(a) shows the X-ray diffraction (XRD) spectra of without coated ABO_w and SiO_2-coated ABO_w calcined at 1100 °C for 1 h, in which tridymite phase can be identified (JCPDS-831832), which shows that the initial xerogel coating has converted to SiO_2. In diffraction patterns of SiO_2-coated ABO_w, no other diffraction peaks were found besides SiO_2 and ABO_w. The presence of diffraction peaks of SiO_2 in the results of coated whiskers confirmed the coating is of SiO_2. This indicates that while fabrication of the preforms, no reactions occur between the SiO_2 coating and ABO_w.

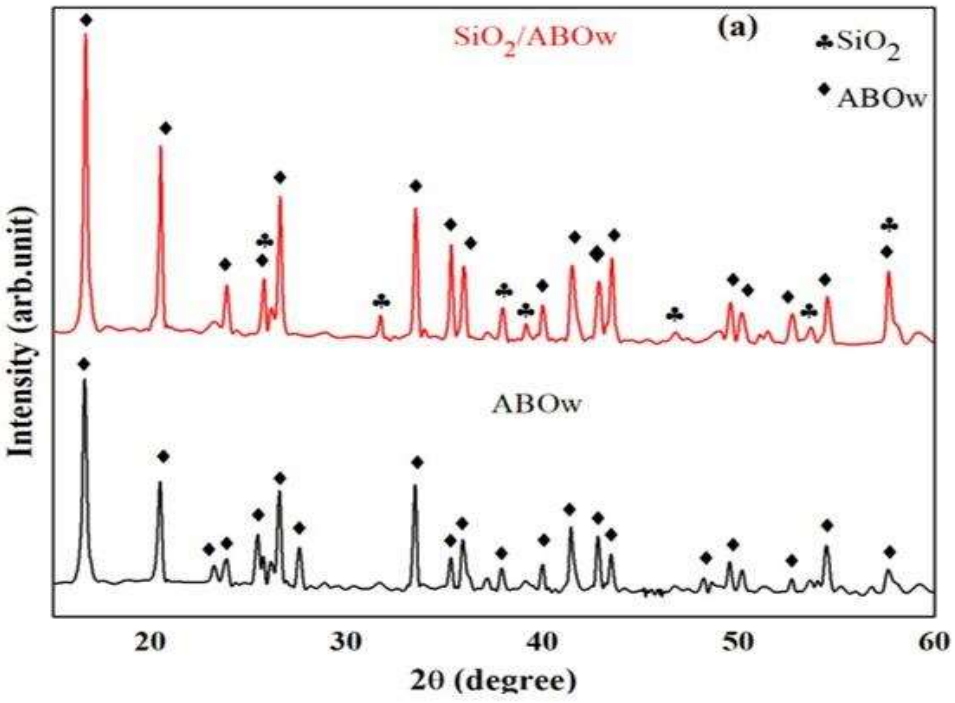

Figure 8.1: (a) XRD spectra of uncoated and SiO_2 coated ABO_w at 1100˚C for 4h

Figure 8.1 (b) shows the XRD patterns of as-cast and composite sample surface which was scanned from 2θ = 20˚ to 2θ = 80˚ with a step size of 0.015˚ at a rate of 5˚C/min. It was found that except SiO_2/ABO_w and Al_2Cu (JCPDS-250012), no other phases were present in the as-cast composites specimen as the volume percentage of SiO_2 coated ABO_w increases in S2, S3, S4, S5, the height of aluminium alloy peaks decreases, whereas the height of coated ABO_w peaks increases, respectively.

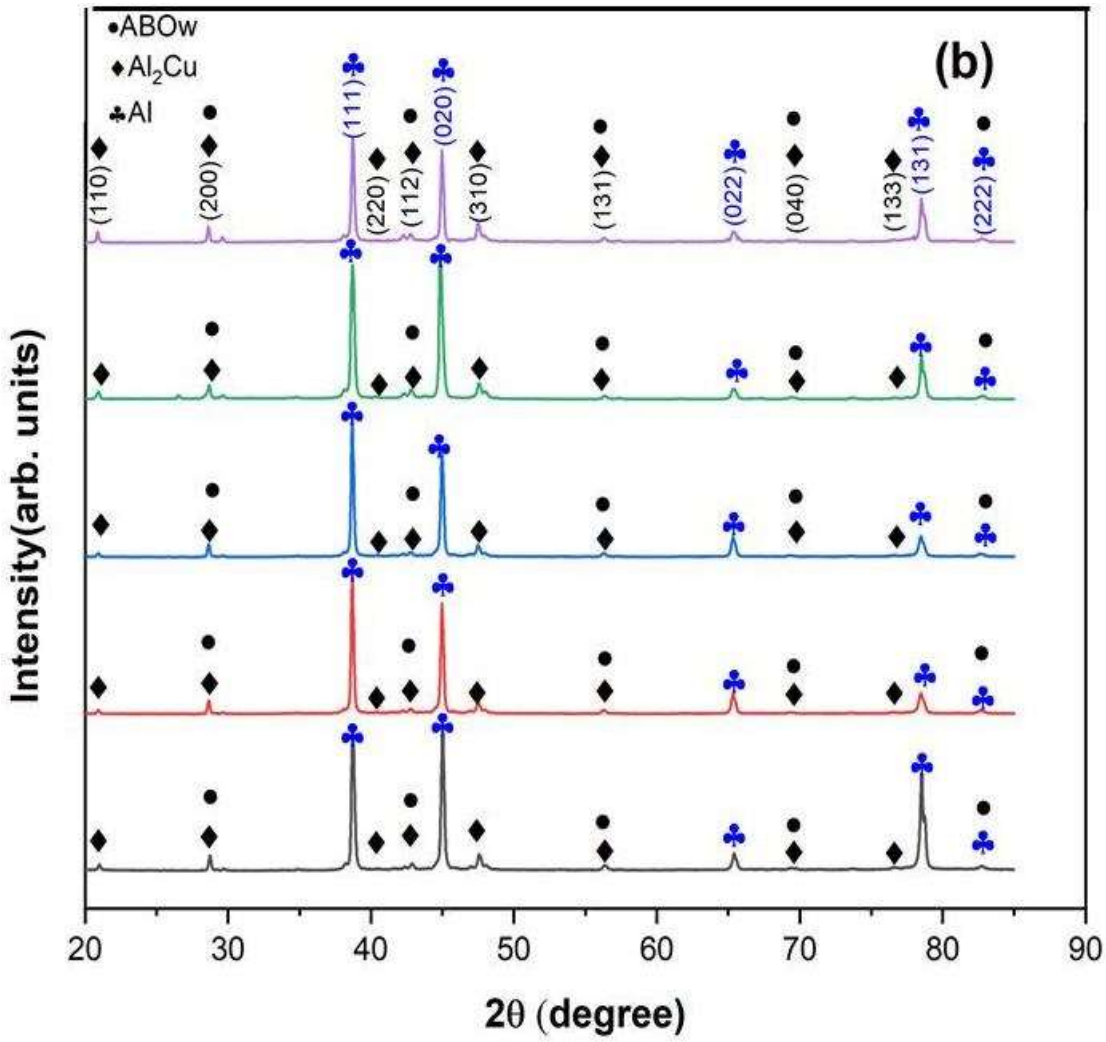

Figure 8.1: (b) Composite samples with different volume fractions of SiO_2 coated ABO whiskers

8.2. Microstructure of the fabricated composites

8.2.1 Scanning electron microscopy

Figure 8.2 is the SEM micrograph of uncoated and SiO_2 - coated ABO_w calcined at 1100 °C for 1h. As seen in **Figure 8.2(a)**, the surface of the uncoated ABO_w is clear and smooth. After coating and calcining, a layer of SiO_2 film is coated on the surface of ABO_w, as shown in **Figure 8.2(b)**. As the coating layer is 30-50 nm, the coating is uniform, as discussed in previous chapter 7. At high-resolution SEM in **Figure 8.2(c)** SiO_2 particles can be seen. The chemical composition measured by EDS is shown in **Figure 8.2(d)**. In a specific region, Al, B, Si, and O were detected. It further confirms from **Figure 8.2 (e)** that the nanoparticles on the surface of ABO_w are SiO_2.

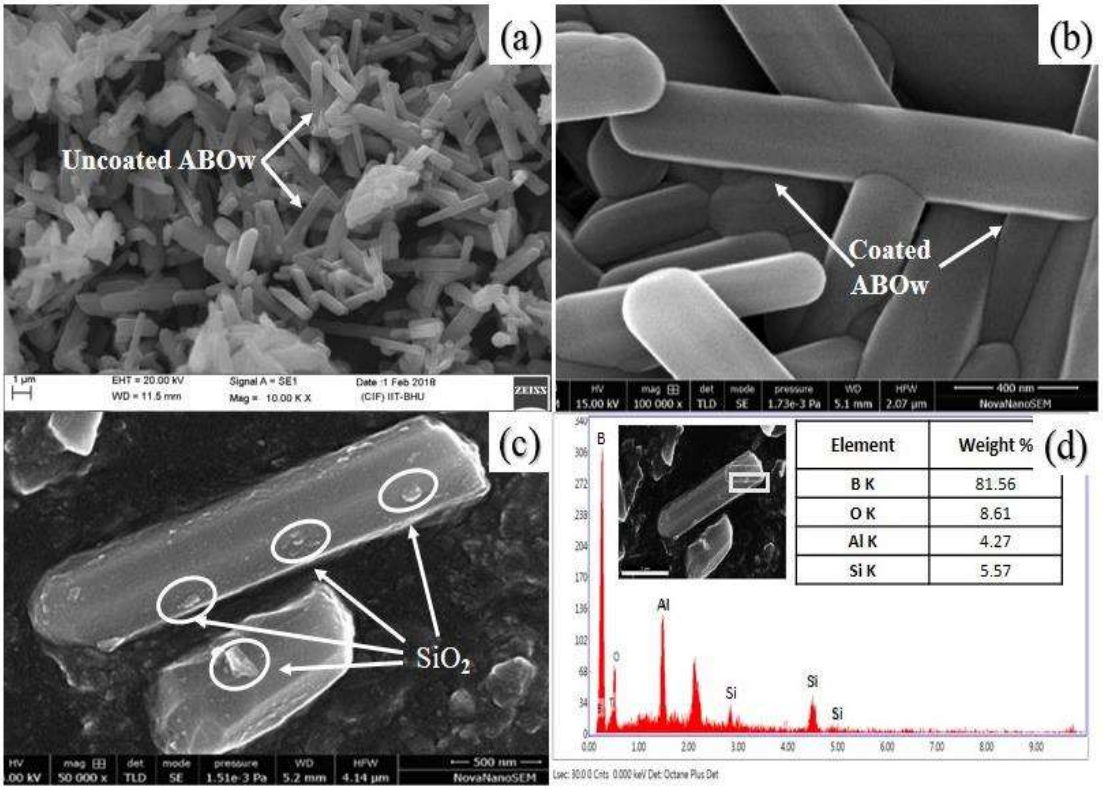

Figure 8.2: SEM micrographs of **(a)** uncoated and **(b)** SiO_2-coated ABO whiskers respectively **(c)** High-resolution SEM of SiO_2 coated whisker **(d)** EDS of SiO_2 coated ABO_w

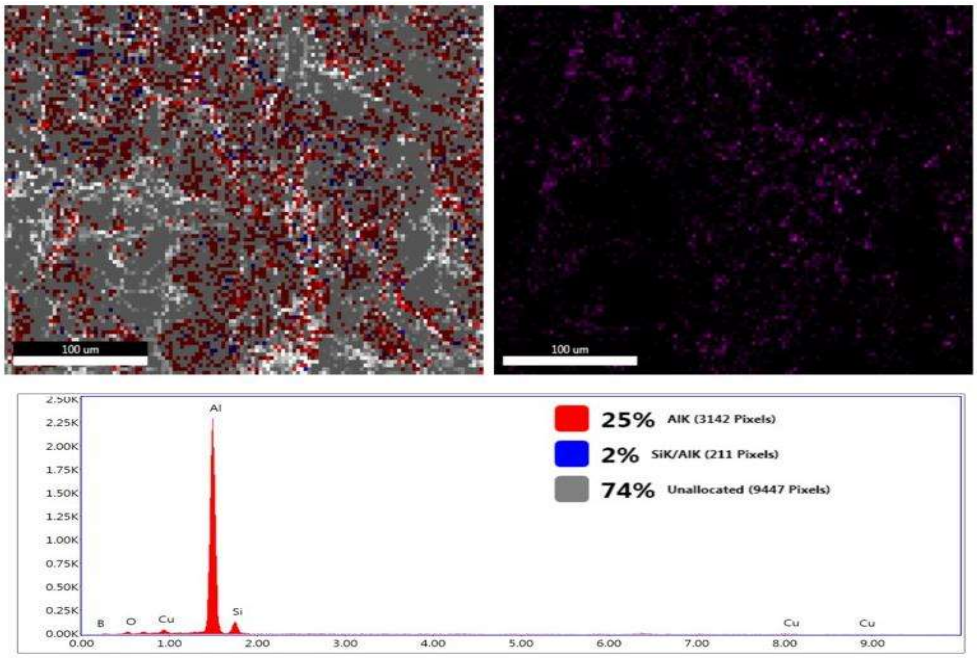

Figure 8.2 (e) Mapping of SiO_2 coated ABO_w reinforced Al-319 composite

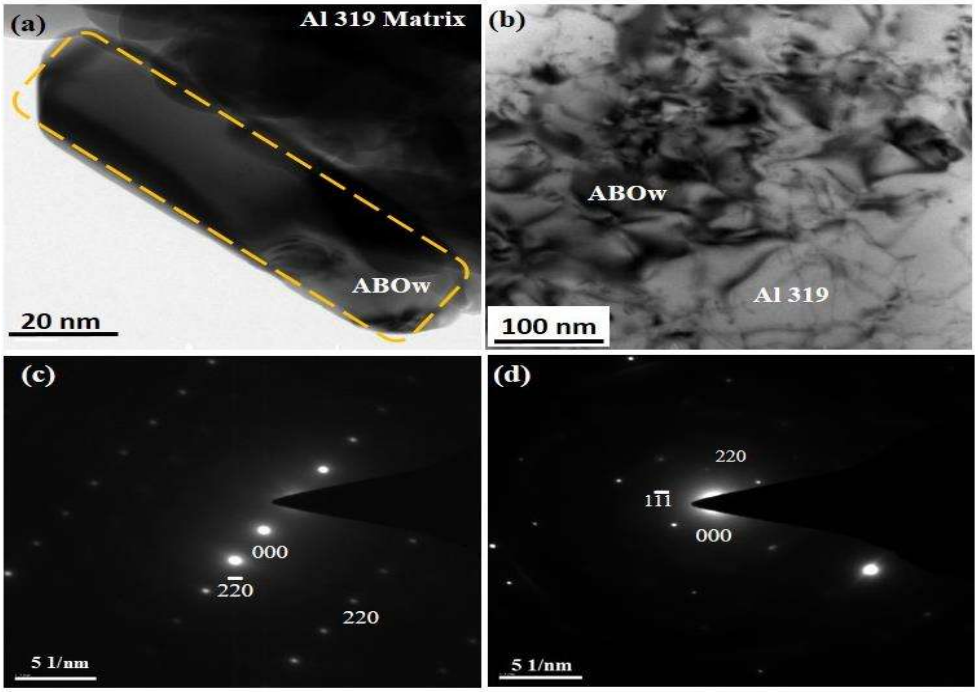

Figure 8.3: TEM micrographs of the interface of **(a)** composite uncoated sample S2 **(b)** ABO_w in Al-319 matrix **(c)** corresponding SADP of composite **(d)** SADP of ABO_w in Al-319 Composite

8.2.2 Transmission electron microscopy

TEM micrographs of the interface in as-cast (ABO_w/Al-319) composites are shown in **Figures 8.3** and **8.4**. The surface of the uncoated whisker is clear and smooth (**Figure 8.3 (a)**). It was seen that it is a single crystal on indexing its (whisker) selected area's electron diffraction pattern (SADP) (from the previous chapter). In **Figure 8.3 (b)**, It can be found that $MgAl_2O_4$ phase forms near the ABO_w/Al-319 composite interface [63].

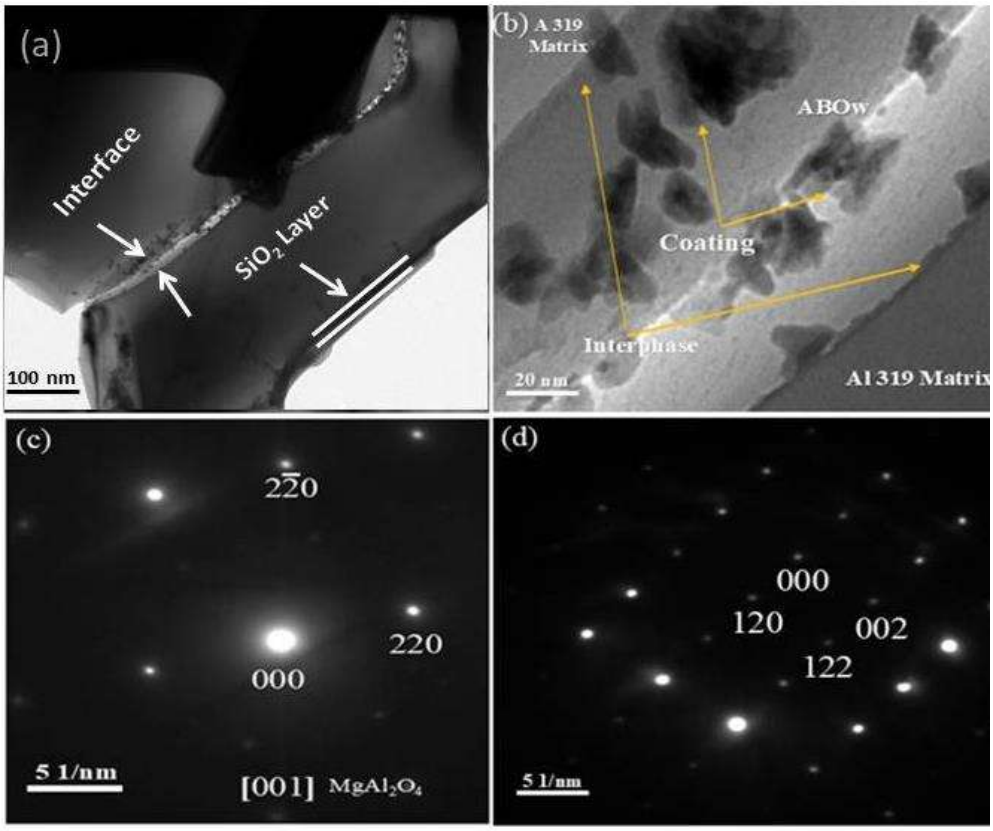

Figure 8.4: TEM micrographs of the interface of **(a)** composite coated sample S2 **(b)** SiO_2 coated ABO_w in A-319 matrix **(c)** corresponding SADP of composite **(d)** SADP of SiO_2 coated ABO_w in Al-319 composite

In case of coated Al-319 composite in **Figure 8.4**. Some fine particles are observed on the surface of whiskers after coating **(Figure 8.4 (b)**). In ABO_w/Al-319 composite at the interface, sparse distribution of small-sized particles was seen. As the contact time between molten Al-319 and ABO_w is short during compo casting, in the matrix of Al-319, the reaction between magnesium and Al-319 is not evident at high temperatures. However, a distribution of continuous product is seen, in SiO_2 /ABO_w /Al-319 composite, at the interface between Al-319 matrix and ABO_w. It was known that it is made of $MgAl_2O_4$ on indexing its selected area's electron diffraction pattern (SADP). Thus, the interfacial reactions (**Eq-8.1-8.4**) during compo casting may be as follows:

$$4Al + 3SiO_2 \rightarrow 2Al_2O_3 + 3Si \quad (8.1)$$

$$2Mg + SiO_2 \rightarrow 2MgO + Si \quad (8.2)$$

$$MgO + Al_2O_3 \rightarrow MgAl_2O_4 \quad (8.3)$$

$$3Mg + 4Al_2O_3 \rightarrow 3MgAl_2O_4 + 2Al \quad (8.4)$$

According to the Al-Si phase diagram, the reactions are at high temperatures [136]. In addition, MgO is not observed, so the formation of $MgAl_2O_4$ may be the reactions **(8.3)** and **(8.4)**. During compo casting at high temperature, the reaction products, Al and B, can dissolve easily into aluminium matrix. As observed in TEM, whiskers were not damaged, and interfacial reactions occurred mainly between aluminium matrix and SiO_2 coating in the composite.

8.3 Mechanical properties of fabricated ccomposites

8.3.1 Tensile properties

The stress-strain curves of the ABO_w/Al-319 composite and SiO_2/ABO_w/Al-319 composites with different ABO_w contents in the alloy are presented in **Figure 8.5 (a)** ABO_w/Al-319 **(b)** SiO_2/ABO_w/Al-319.

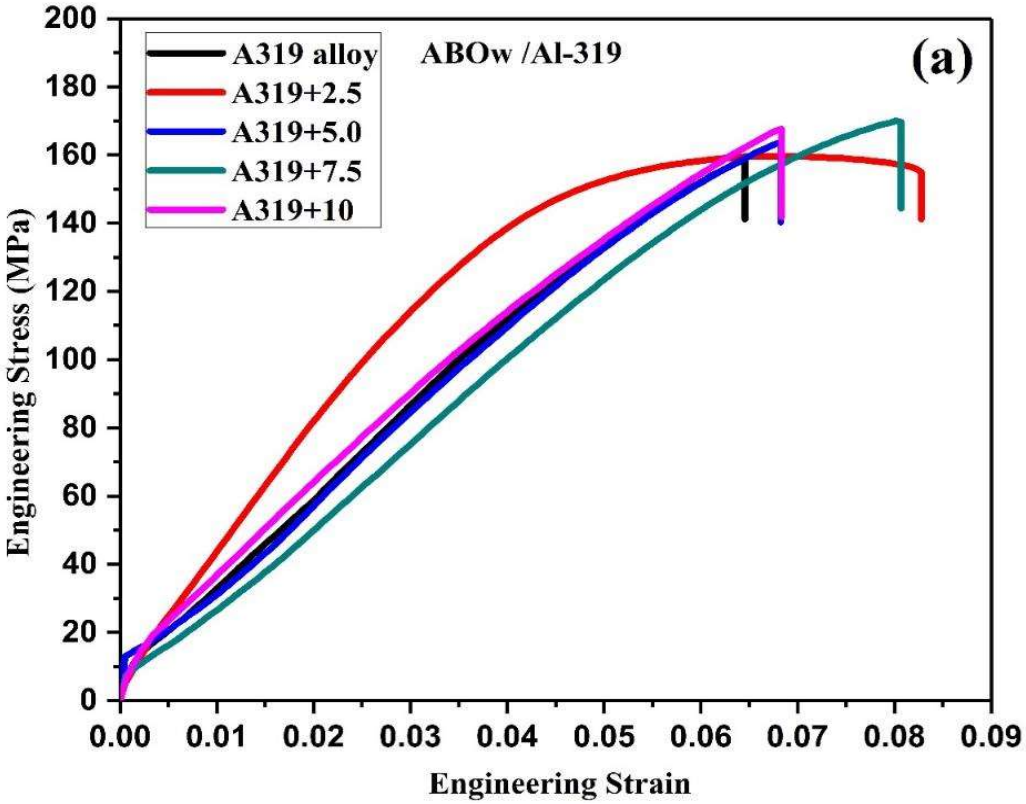

Figure 8.5: (a*)* Engineering stress – strain curve Al-319 base alloy and ABO_w/Al-319 composites

It can be seen that the tensile properties of composites enhanced significantly by the application of SiO_2 coating on ABO whiskers. An improvement in tensile strength was observed in SiO_2/ABO_w/Al-319 composite compared to ABO_w/Al-319 composite without SiO_2 coating. Also, the elongation to fracture (δ), the elastic modulus, and elongation yield strength were seen to be improved, as shown in **Table 8.1**.

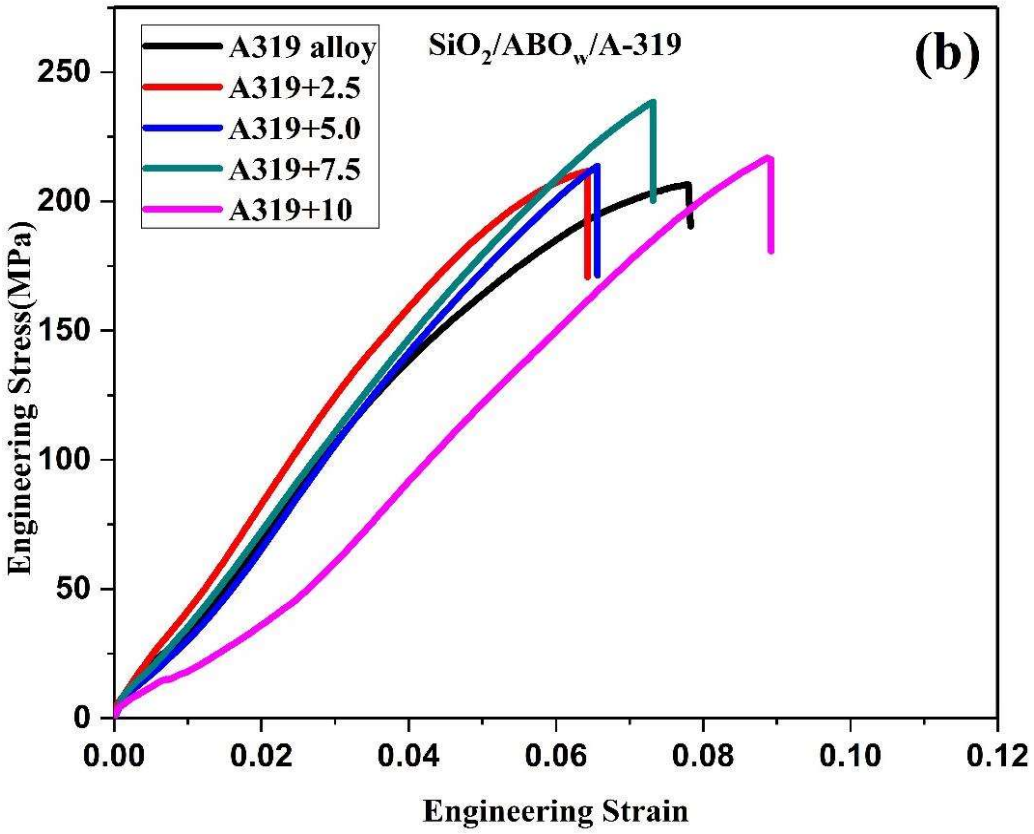

Figure 8.5: (b) Engineering stress-strain curve Al-319 alloy and SiO_2 /ABO_w/Al-319 composites

Table 8.1: Mechanical properties of fabricated alloys

Alloys	YS		UTS		El (%)	
	ABOw	SiO_2 Coated ABOw	ABOw	SiO_2 Coated ABOw	ABOw	SiO_2 Coated ABOw
S1 (Al-319)	89	92	158	160	6.1	6.2
S2 (2.5 %ABO_w/Al-319)	98	115	159	211	5.0	5.3
S3 (5.0%ABO_w/Al-319)	95	121	163	213	5.2	5.8
S4 (7.5%ABO_w/Al-319)	103	123	170	238	5.9	6.4
S5 (10%ABO_w/Al-319)	101	119	167	216	5.4	6.1

8.3.2 Fracture morphology of composites

The tensile fracture surfaces of the Al-319 alloy composites **(Figure 8.6)** reinforced with varying percentages (2.5, 5, 7.5, 10 wt.%) of uncoated ($Al_{18}B_4O_{33}$) ABO whiskers are presented in **Figure 8.7 (a), (b), (c)** and **(d)** and with higher magnification (10000 X) in **Figure 8.8**. It can be seen as the fractography of base alloy

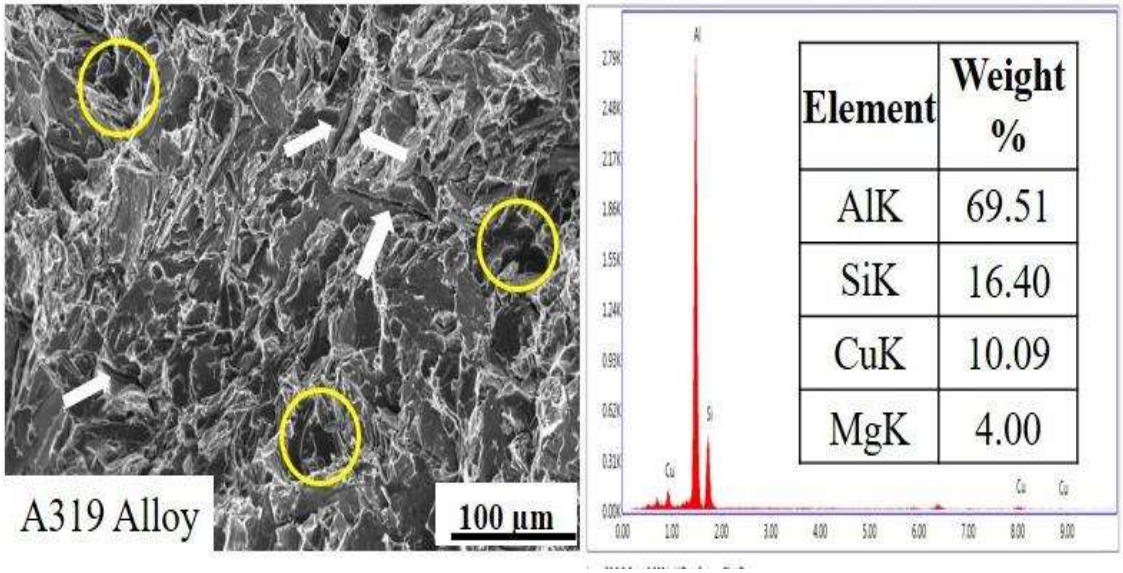

Figure 8.6: Tensile fractography of the as cast A-319 base alloy with EDS spectrum in a specific region

it consist of a few dimples and micro-cracks (encircled), which represent the ductile nature of the fracture. **Figure 8.7 (b)** and **(c)** shows the fracture behavior of 2.5 and 5 % ABO_w/Al-319 composite consists of fracture of whiskers, pull-out, and dimples. The pull-out and fracture of circled whiskers are shown at higher magnification in **Figure 8.8 (a)** and **(b)**. It may result from the unfilled regions of molten aluminium created during the tensile deformation by the interfacial debonding (detachment) between matrix and whisker or during the casting process by poor ABO_w/aluminium wettability. The UTS of the composite is low due to the weak interfacial bonding [138].

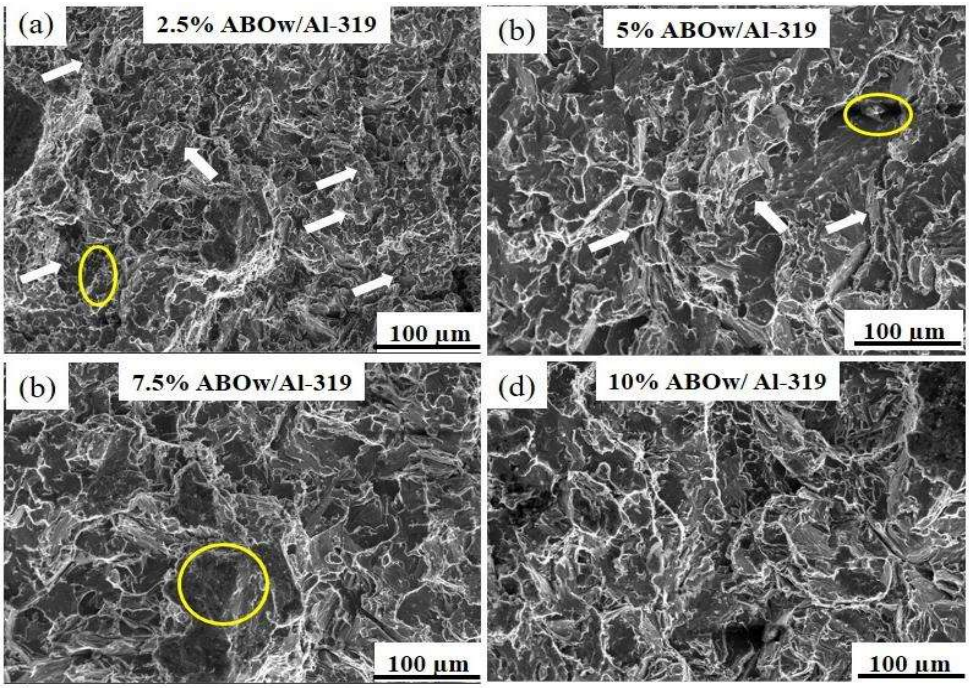

Figure 8.7: Tensile fractrograph of the ABO_w/Al-319 composites containing **(a)** 2.5%ABO_w **(b)** 5%ABO_w **(c)** 7.5% ABO_w **(d)** 10% ABO_w

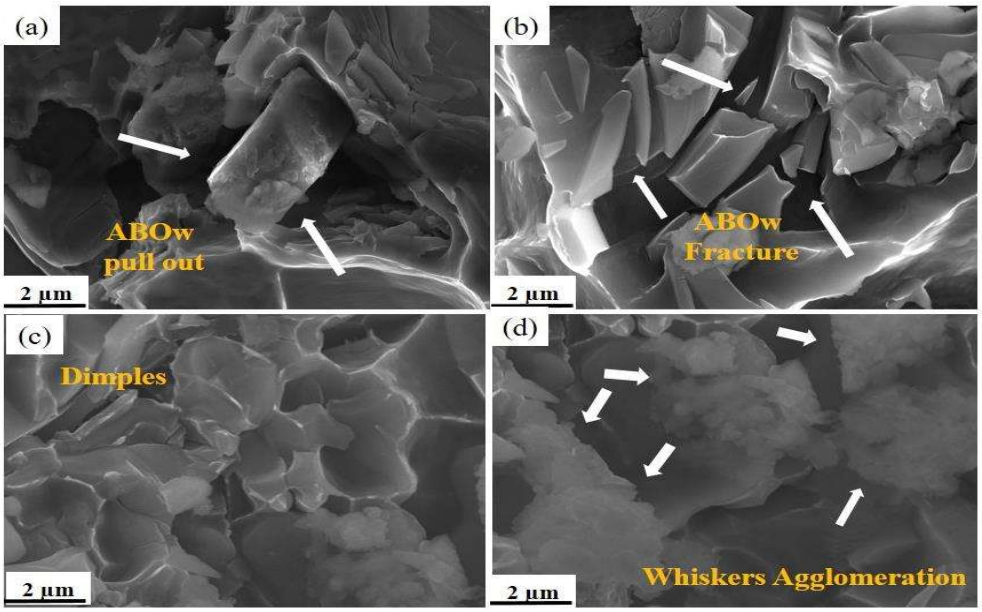

Figure 8.8: Higher magnification (10000x) tensile fractrograph of the encircled region ABO_w/Al-319 composites (from figure 8.6) containing **(a)** 2.5%ABO_w **(b)** 5%ABO_w **(c)** 7.5% ABO_w **(d)** 10% ABO_w

A great deal of dimples appear in 7.5%ABO_w/Al-319 (**Figure 8.7 (c)**), the matrix has good plastic deformation capability, which is in confirmation with the tensile stress-strain curve of the ABO_w/Al-319 composite and micrograph at higher magnification **Figure 8.8 (c)** in a specific region. The fractography of the composite has dimple and cleavage fracture in few areas, which indicates a high bonding strength between the matrix and whisker in the 7.5% ABO_w/Al-319 composite. Ductile fracture of matrix leads to more small dimples as found on the fractography. In addition, the presence of the high content (10 wt%) of ABO_w, agglomeration of whiskers (Higher magnification in **Figure 8.8 (d)**) leads to reduced UTS of composite as the load-transfer capability from matrix to whisker decreases.

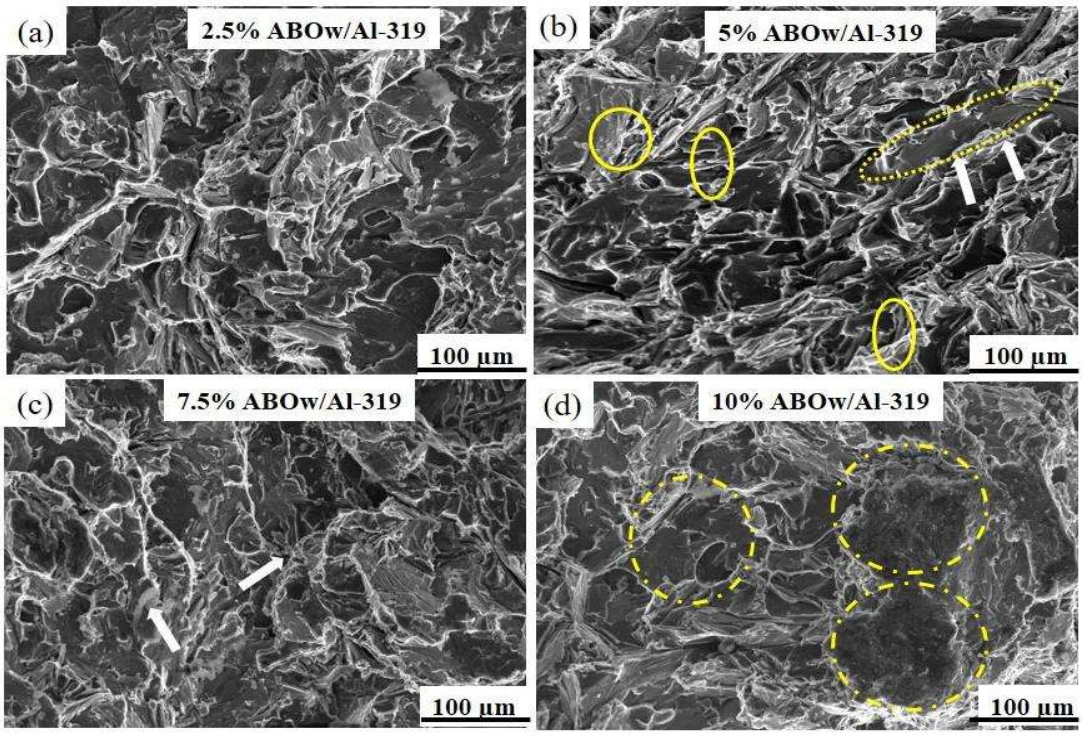

Figure 8.9: Tensile fractrograph of the SiO_2/ABO_w/Al-319 composites containing **(a)** 2.5% ABO_w **(b)** 5% ABO_w **(c)** 7.5% ABO_w **(d)** 10% ABO_w

The fracture micrograph of SiO_2/ABO_w/Al-319 composite after the tensile test is shown in **Figure 8.9**. As mentioned above, the microstructure at the ABO_w/Al-319 composite interface changes due to whisker coating with SiO_2. After whisker coating, an improvement in whisker/matrix interface bond and prevention of interfacial reaction and whisker damage is expected [139].

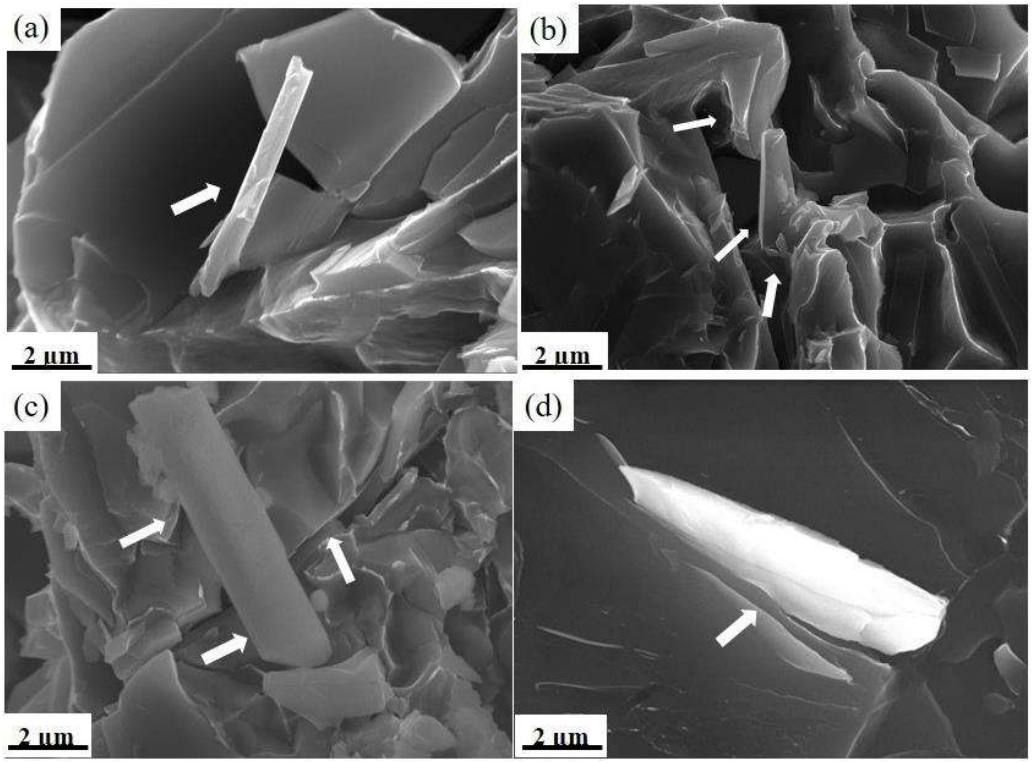

Figure 8.10: Higher magnification (10000x) tensile fractrograph of the encircled specific region of SiO_2/ABO_w/Al-319 composites containing (a) 5% ABO_w (b) 7.5% ABO_w without dimples (c) 7.5% ABO_w crack impedement by whisker (d) 10% ABO_w

Figure 8.9 (a) and **(b)** represents fracture morphology of the coated whiskers reinforced 2.5 and 5% ABO_w/Al-319 composite. The resistance of pull-out of whiskers and interfacial bonding strength increases with coating content (5% coated ABO_w) in **Figure 8.10 (a)**. The tensile fractography of the SiO_2/7.5% ABO_w/Al-319 composite is

shown in **Figure 8.9 (c)**; fracture of whiskers and pull-out can hardly be seen. Moreover, there are almost no dimples in the matrix (higher magnification) in **Figure 8.10 (b)),** and in fractography some cracks are found as indicated at higher magnification in **Figure 8.10(c)** which might be impeded by a coated whisker. In SiO_2/10%ABO_w/Al-319 composite, more and larger dimples are seen (encircled in **Figure 8.9 (d)**), and due to the pull-out of whiskers, the remaining hole is rougher (**Figure 8.10 (d)**). The matrix to whisker load transfer capability at the interface decreases due to the high content of coated ABO_w, leading to reduced UTS of the composite.

8.4. Dry sliding wear behaviour

8.4.1 (a) Effect of sliding distance on weight loss-

It is observed from **Figure 8.11 (a)** that with increasing the sliding distance, the weight loss increases in all composites and base alloy. But it can be seen that the weight loss for composite with 7.5% and 10% ABO_w start decreasing after a sliding distance of 1800 m. During sliding wear, the propagation of cracks is resisted by interactions between ABO_w particles and dislocations. Coefficient of thermal expansion mismatch during solidification leads to the formation of strain field surrounding the reinforced particles that resist the crack propagation while sliding and subsequent material removal. Enhanced wear resistance is obtained due to delayed detachment of particles from aluminium matrix caused by good reinforcement/matrix bonding and better interface [140].

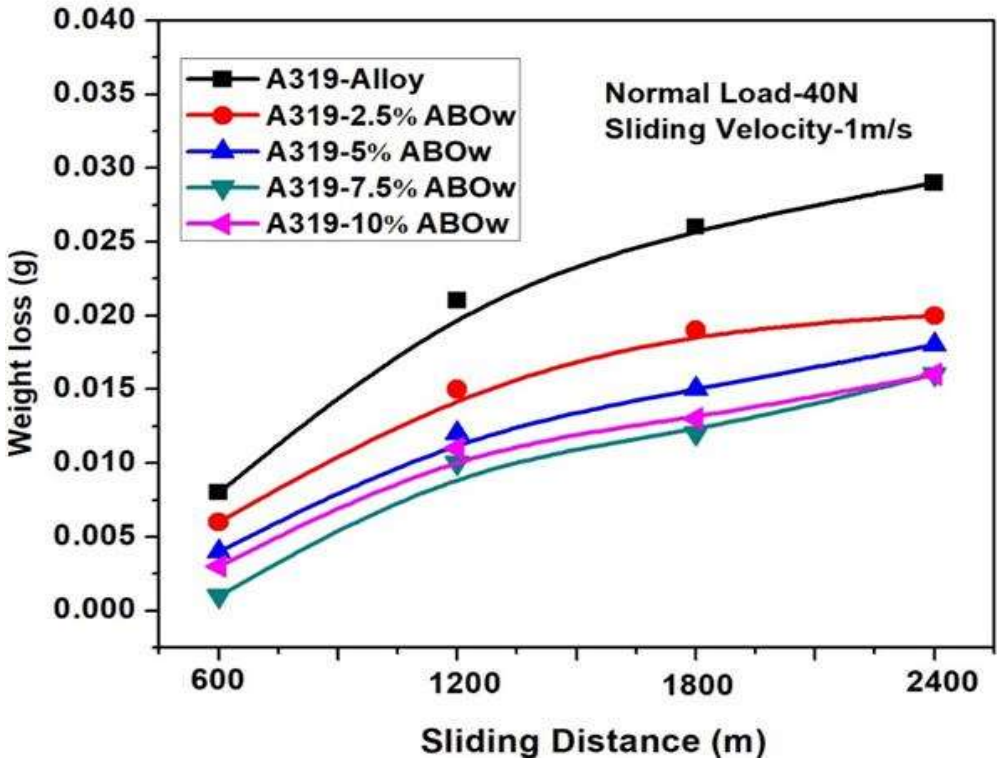

Figure 8.11: (a) Variation of weight loss with the sliding distance of alloy and composite

8.4.2 (b) Effect of sliding distance

Figure 8.11 (b) shows the effect of sliding distance on the coefficient of friction of alloy and composites at an applied load of 40 N and sliding velocity of 1m/s. The curve of composite reinforced with 10% ABO_w is stable compared to other materials under observation. The increased percentage of SiO_2 coated whiskers in the matrix has improved its wettability, providing a mechanically stable surface for the applied load. Thus the composites with an increasing 7.5 to 10 wt percentage of whisker reinforcement show a better coefficient of friction as compared to alloy.

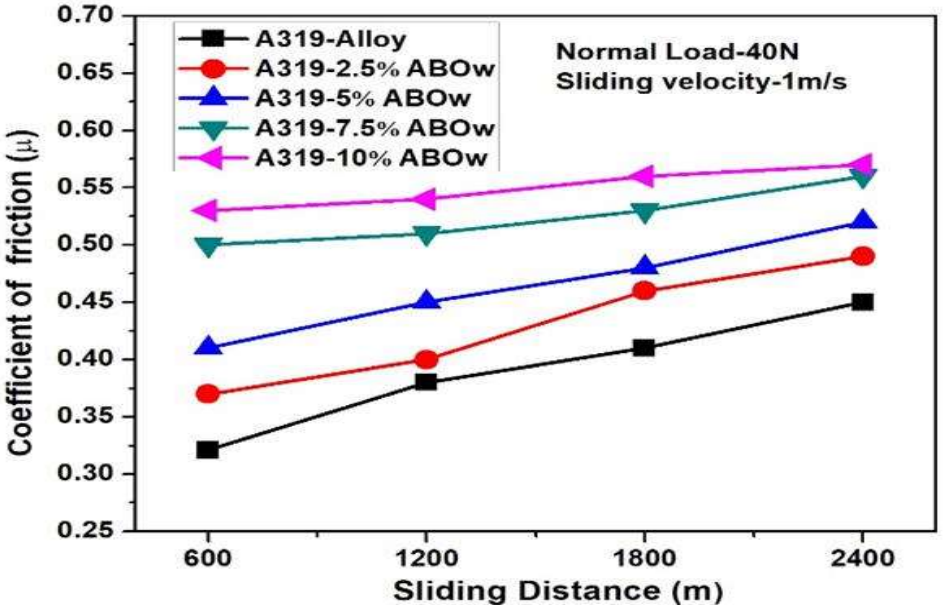

Figure 8.11:(b) Variation of COF with the sliding distance of alloy and composite

8.4.3 (c) Effect of applied load

It is observed from **Figure 8.11 (c)**, the wear rate increases linearly with an increase in the applied load.

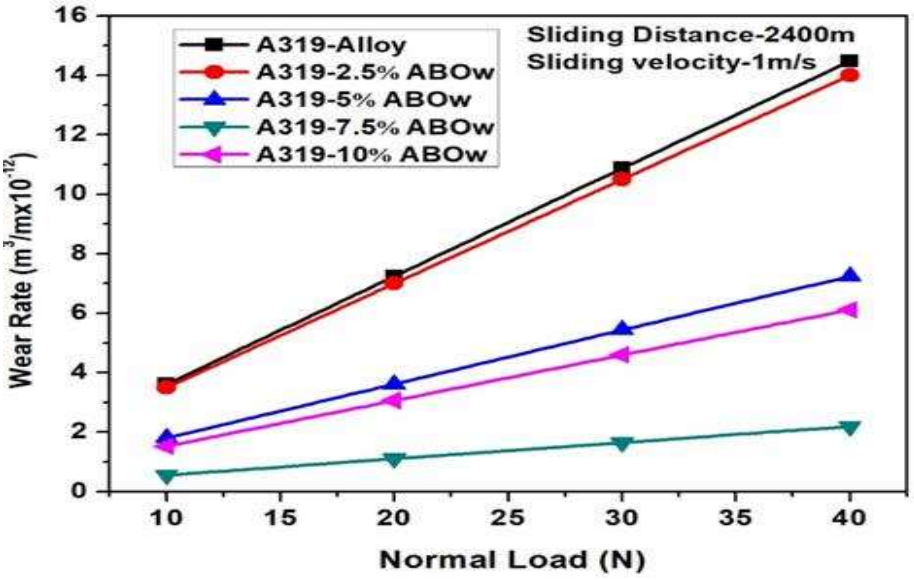

Figure 8.11: (c) Variation of wear rate and normal load of alloy and composite

This increase in wear rate is due to frictional heat generated during the dry sliding wear test [141-144]. The frictional heat develops due to surface contact of pin and disc. However, more frictional heat produces at a high load, and the corresponding wear rate may be increased. An increase in normal load leads to an increase in micro-cracking at the surface. SEM analysis of the worn surface of the alloy and composites in **Figure 8.8 (c)** show the delamination, shallow plough, wear debris, and morphology of the friction surfaces indicate that micro-cracks and holes appear on the worn surface with increasing load.

8.4.4 Analysis of wear and friction

It was increasing the coated SiO_2 /ABO_w in the alloy increased the hardness and oxide layer formation at the surface. This is why the SiO_2 /ABO_w /Al-319 exhibits a fairly good wear resistance.

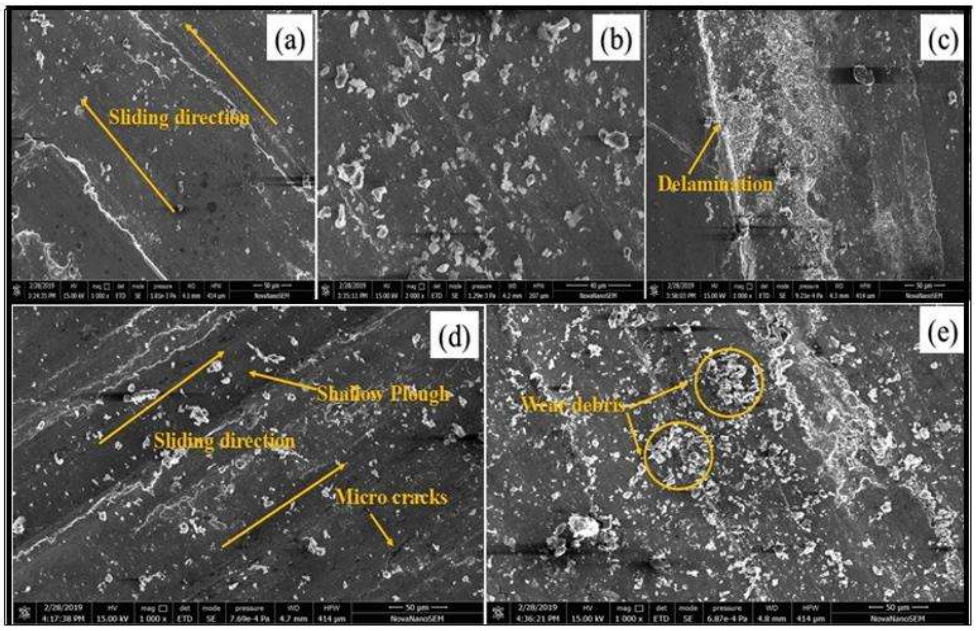

Figure 8.12: SEM micrographs of worn surfaces with load variations **(a)** As cast (Al-319 alloy) **(b)** 2.5 % coated ABO_w/Al-319 **(c)** 5% coated ABO_w/Al-319 **(d)** 7.5% coated ABO_w/Al-319 **(e)** 10% coated ABO_w/Al-319

The oxygen weight percentage varies during dry sliding contact, as shown in **Figures 8.12 (a-d);** this is because high frictional heat developed between counterface and pin. It also shows the worn surfaces for the analysis of wear debris and oxide layer. The oxide layer created on the surface may affect the wear resistance properties, which act as a protective layer and decrease the wear rate [145-148]. However, oxidative and abrasive wear is mainly involved in the case of composites without any seizing wear [149]. The higher percentage addition of reinforcement (10% coated ABO_w) forming larger quantities of debris, which increases the wear rate (**Figure 8.12 (d)).** It might be due to non-uniform distribution or agglomeration of whiskers at the surface.

8.4.5 Characterization of the worn surfaces

Figure 8.13 shows the EDS of alloy and composites. EDS detected aluminium, copper, silicon, magnesium, and Fe traces in the surface's wear analysis processed at 2400 rpm with 40 N load **Figure 8.12(a)**.

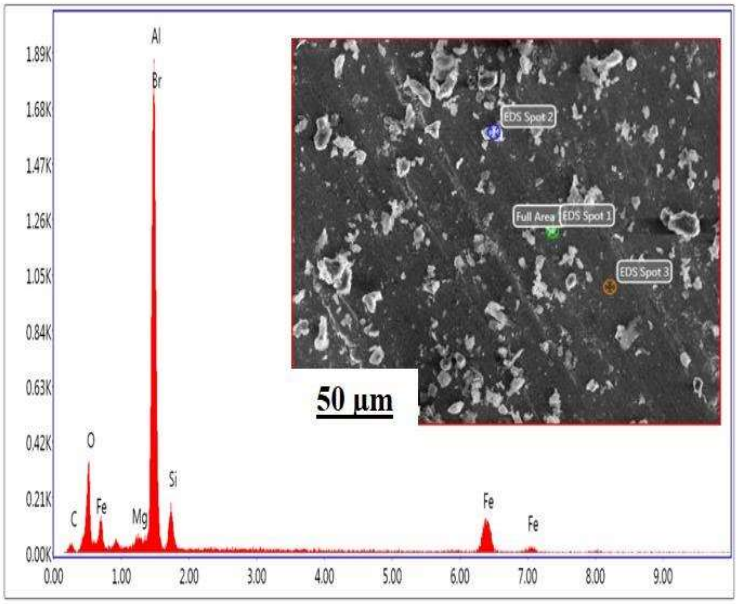

Element	Weight %
C K	7.54
O K	17.00
Mg K	0.98
Br L	15.53
Al K	28.39
Si K	4.77
Fe K	25.79

Figure 8.13: (a) EDS spectrum (elemental analysis) of Al- 319 alloy

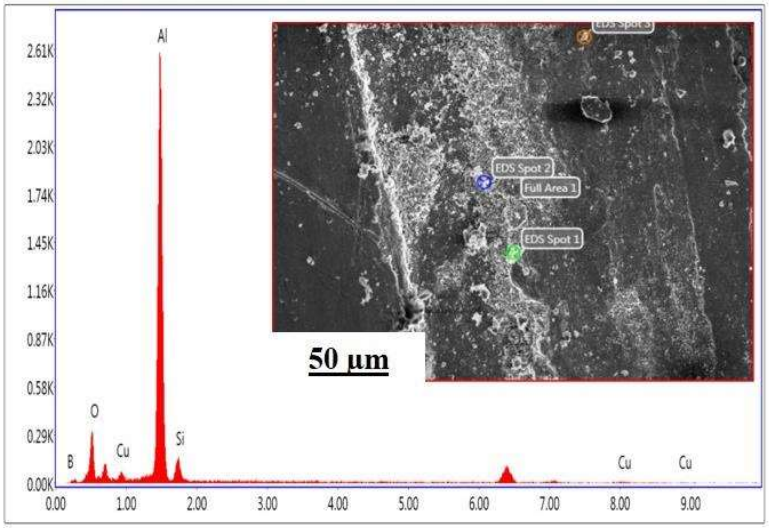

Element	Weight %
B K	25.92
O K	28.60
Al K	40.83
Si K	1.82
Cu K	2.83

Figure 8.13: (b) EDS spectrum in respect of SiO_2 coated 2.5% ABO_w/ Al-319 alloy

Figure 8.13 (b), (c), and **(d)** shows the EDS spectrum in respect of increasing the percentage of ABO_w the boron presence enhances the agglomeration as boron does not mix in a short time in the aluminium matrix during semi-solid or compo casting.

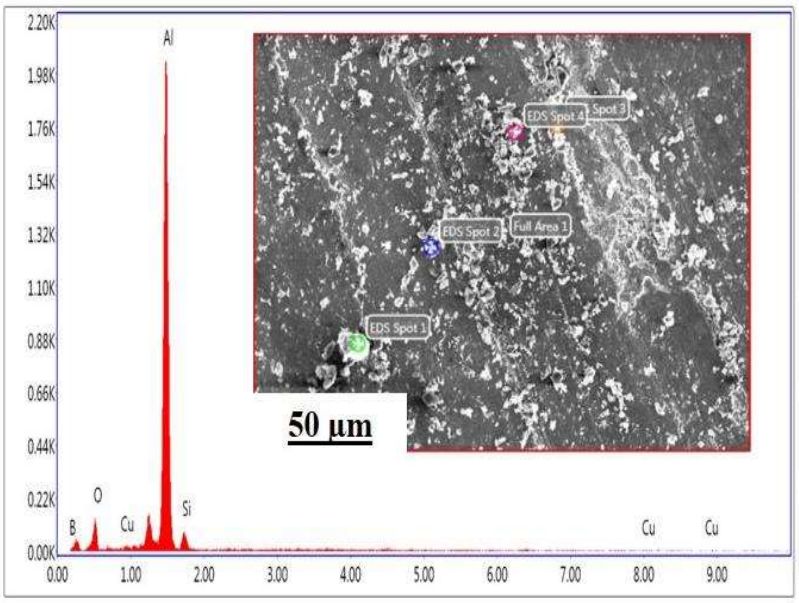

Element	Weight %
B K	42.32
O K	9.07
Al K	44.75
Si K	2.32
Cu K	1.54

Figure 8.13: (c) EDS spectrum in respect of SiO_2 coated 5.0% ABO_w / Al-319 alloy

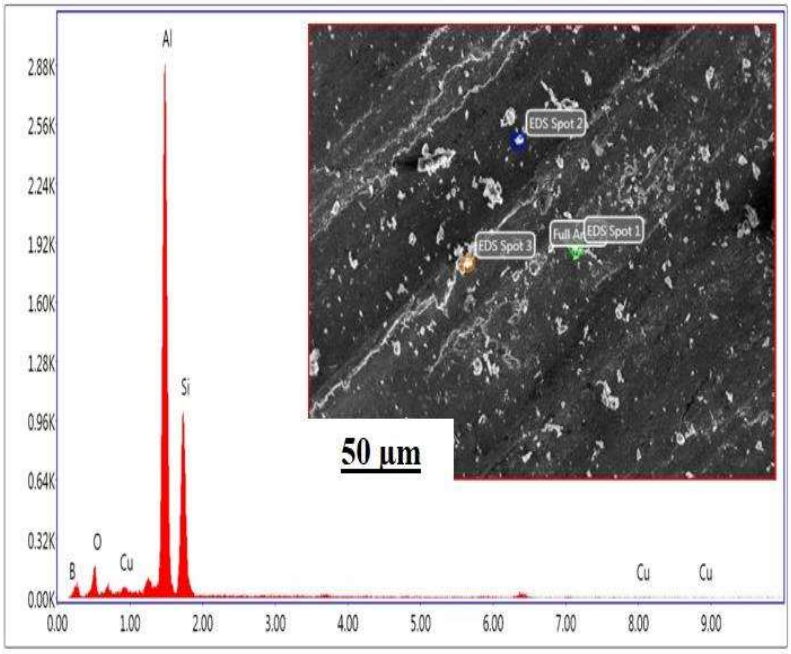

Element	Weight %
B K	66.06
O K	17.80
Al K	14.37
Si K	0.99
Cu K	0.78

Figure 8.13: (d) EDS spectrum in respect of SiO_2 coated 7.5.% ABO_w/ Al-319 alloy

8.5 Scratching, wear, and fabrication studies

Surface topography is another method used to evaluate surface quality after the wear test. For the surface topography, atomic force microscopy (AFM) was used. This characterization is done on the worn surface of the materials for quantitative analysis of its roughness in terms of root mean square deviation of profile (Rq) and arithmetical mean deviation of profile (Ra). **Figures 8.14** and **8.15** show 2D images and topography maps (3D image) of the worn surfaces under alloy and four composites. 3D profiles of worn surfaces show the peak height and depth of the valley with different colours [150].

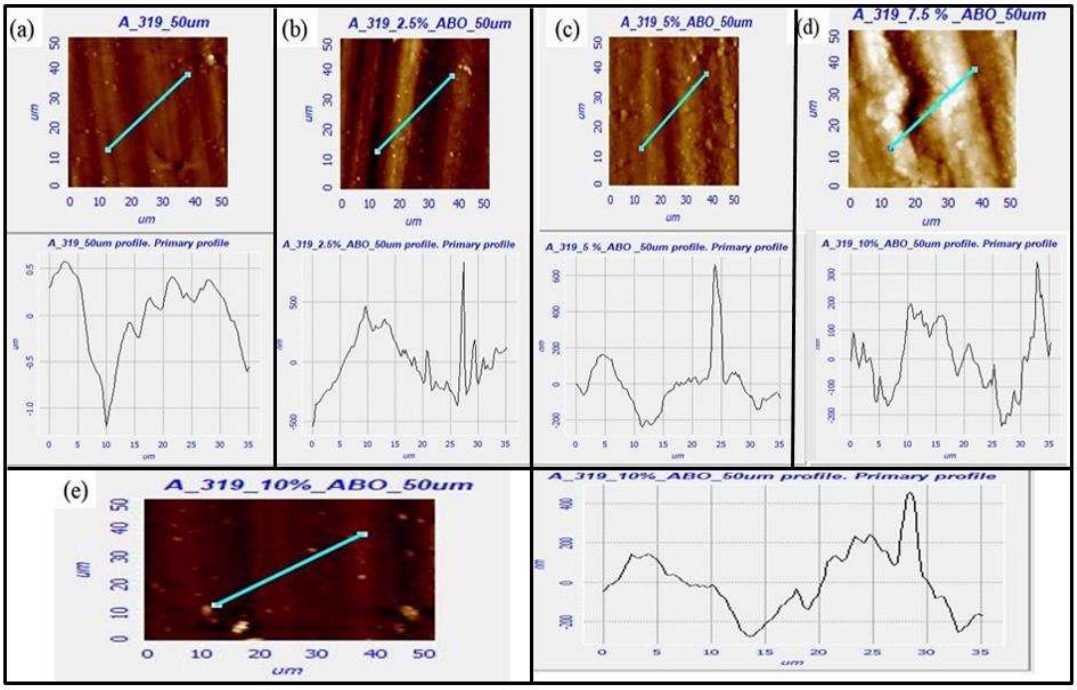

Figure 8.14: Line analysis results perpendicular to wear track and 2D-profilometric images of (a) as cast (Al-319) and coated ABO_w containing (b) 2.5% ABO_w (c) 5% ABO_w (d) 7.5% ABO_w (e) 10% ABO_w

Table 8.2 Roughness parameters of worn surfaces of alloy and composite

Roughness (µm)	S1	S2	S3	S4	S5
R_{max}	1.789	1.389	0.821	0.592	0.791
R_p	0.579	0.845	0.456	0.352	0.542
R_v	1.21	0.64	0.274	0.274	0.238

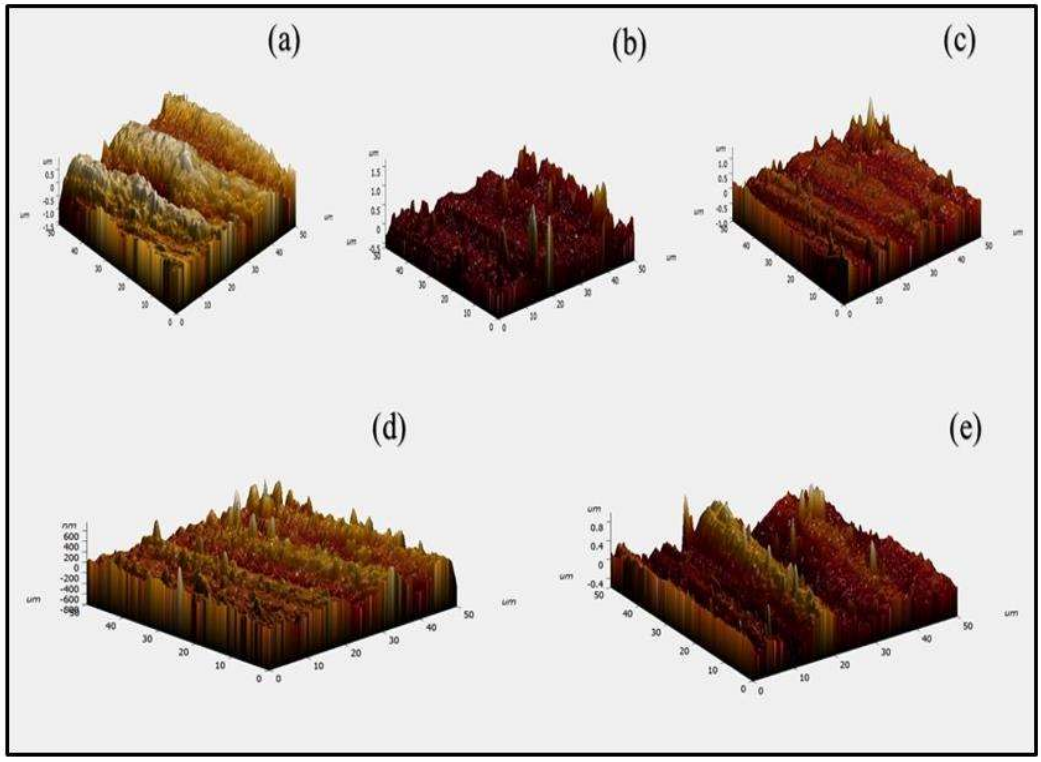

Figure 8.15: 3D tropography of the worn surface of devloped materials (a) Al-319 as cast alloy **(b)** composite containing 2.5wt % ABO_w **(c)** 5wt% ABO_w **(d)** 7.5 wt% ABO_w **(e)** 10wt% ABO_w

From **Table 8.2**, The surface roughness is maximum in alloy and minimum with 7.5 wt.% coated ABO_w and increases a little bit with 10 wt.% coated ABO_w. The minimum roughness observed is in agreement with the observed higher weight percentage of coated ABO_w phases in these regions. For the topography map selected region gives more rough regions rather than the randomly selected region.

8.6 Chapter summary

By hydrothermal synthesis, the $Al_{18}B_4O_{33}$ whiskers can be successfully coated with SiO_2. During compo-casting, the molten A-319 alloy reacts with SiO_2 coating on alumina borate whiskers (ABO_w), thus forming a uniform layer of $MgAl_2O_4$ at the interface. The interfacial reactions can be reduced by surface treatment of the whiskers.

The UTS and δ of the composites also get affected by interfacial reactions due to SiO_2 coating on whiskers in ABO_w/Al-319 composites. The UTS and δ of the composites first increase and then decrease with increased coated ABO_w content. The composite with optimum coated ABO_w content (SiO_2/7.5%ABO_w/Al-319 composite) attained the maximum value of the UTS (238 MPa) and δ (6.4%). The tensile fractography of the SiO_2/7.5%ABO_w/Al-319 composite also shows fracture and pull-out of whiskers is hardly seen and whiskers impede cracks.

The wear resistance of the aluminium composite is significantly improved due to the Al_2O_3 formation and ABO_w particles under present scratch test conditions. However, with 10% coated ABO_w, non-uniform distribution forms larger quantities of debris. An increase in coefficient of friction and wear rate was induced under low load on increasing the sliding speed that causes deep surface damage. A decrease in coefficient of friction and wear rate occurs due to oxide transfer layer formation on the worn surface and strain hardening of the subsurface layer, increasing the sliding speed further. Slight plastic deformation and adhesion wear were also seen on worn surfaces along with oxidation wear. On increasing the applied load the friction coefficient and wear area of the samples increases almost linearly. As sliding distance affects the coefficient of friction and wear in this study, no regular change is found in the 7.5-10% coated ABO_w/Al-319 composite.